A Platinum Open Access Journal for Organic Chemistry

Paper

Free to Authors and Readers

DOAJ Seal

Arkivoc **2022**, part iii, 0-0

to be inserted by editorial office

A cascade reaction of imidazo[1,2-*a*]pyridines with maleic anhydride: Formation of cross-conjugated mesomeric betaines

Chandani Mathur,[a] Raakhi Gupta,[a]* Raj K. Bansal,[a] Deepak B. Salunke,[b] and Shailesh W. Gohad[c]

[a] *IIS (Deemed to be University), Jaipur, India - 302020*

[b] *Department of Chemistry, Panjab University, Sector 14, Chandigarh, India - 160014*

[c] *Analytical Research- Macleods Pharmaceuticals Ltd., G-2 Mahakali Caves Road, Shantinagar, Andheri (E), Mumbai, India – 400093*

Email: raakhi.gupta@iisuniv.ac.in

Dedication to Professor György Keglevich on his 65th birthday

Received mm-dd-yyyy **Accepted Manuscript** mm-dd-yyyy **Published on line** mm-dd-yyyy

Dates to be inserted by editorial office

Abstract

In recent years, organic donor-acceptor complexes have attracted much attention, leading to the development of new organic switchable, binary electronic materials with high data-storage capacity. Following addition of a solution of maleic anhydride to a solution of imidazo[1,2-*a*]pyridine(s), a cascade reaction ensues, resulting in the formation of cross-conjugated mesomeric betaines (CCMB), wherein positive and negative charges are restricted exclusively to different parts of the molecule. Physico-chemical properties of the compounds revealed the existence of intramolecular charge-transfer phenomena which could stimulate their interest as potential luminescent materials.

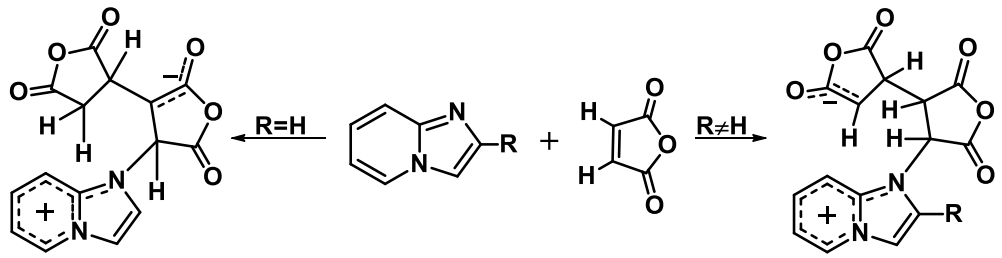

Keywords: Cross-conjugated mesomeric betaine, imidazo[1,2-*a*]pyridines, maleic anhydride, 1,4-dipoles, CT complex, fluorescence

Introduction

Cross-conjugated mesomeric betaines (CCMB) belong to the general class of mesomeric betaines (MB) which are neutral, conjugated molecules, representable only by dipolar structures. Both positive and negative charges are delocalized within the respective π-frameworks. Based on the extent of delocalization of the positive and negative charges, the heterocyclic mesomeric betaines have been classified broadly into three groups: conjugated mesomeric betaines (CMB), cross-conjugated mesomeric betaines (CCMB), and pseudo-cross-conjugated mesomeric betaines (PCCMB). Ylides, which can be represented satisfactorily by a 1,2-dipolar structure, are examples of CMBs. In CCMBs, the positive and negative charges are delocalized exclusively in different parts of the molecule. In PCCMBs, the two charges are delocalized effectively, but not exclusively, in different parts of the molecule.[1] Potts and co-workerssubsequently reported theoretical and experimental results of a variety of CCMBs and PCCMBs incorporating various heterocyclic skeletons.[2] Ramsden highlighted the relationship between heterocyclic mesomeric betaines and isoconjugate alternant and non-alternant hydrocarbon dianions.[3] One example each of CMB, CCMB and PCCMB are shown in Figure 1.

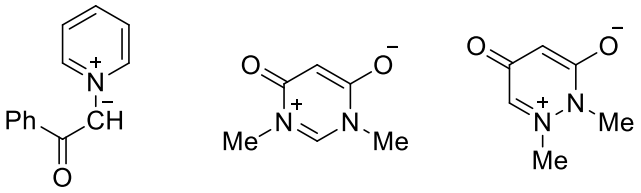

1 **2** **3**

Figure 1. Examples of CMB (1), CCMB (2) and PCCMB (3).

Over the years, interesting applications have been expanded in various fields utilizing these reactive intermediates. For example, Padwa and co-workers developed an efficient stereo-controlled route to the isoschizozygane alkaloid core by using intramolecular 1,4-cycloaddition of a CCMB.[4] Nechaev et al. developed a facile multicomponent synthesis of indolizine-derived PCCMB with high level of functional compatibility making possible the preparation of a number of compounds for materials and medicinal chemistry.[5] These have revealed unique molecular packing and structure-property relationships.

In 1932, Diels and Alder reported a cascade reaction of pyridine with dimethyl acetylenedicarboxylate (DMAD) to yield two products whose structures could not be established at that time.[7] Later, these compounds were identified as tetramethyl-4H-quinolizine-1,2,3,4-tetracarboxylate[8] and tetramethyl-9aH-quinolizine-1,2,3,4-tetracarboxylate.[9] Huisgen and co-workers subsequently rationalized the whole sequence of reactions by postulating an *in situ* generation of a 1,4-dipole from the reaction of pyridine with DMAD, followed by its 1,4-dipolar cycloaddition with a second molecule of DMAD (Scheme 1).[10] It was also emphasized that, in contrast to 1,3-dipoles, 1,4-dipoles can be generated *in situ* only, and cannot be isolated.

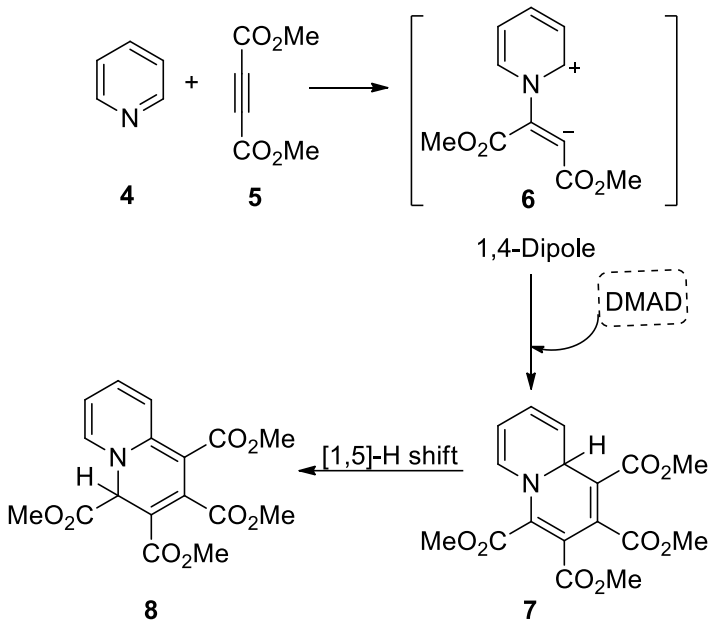

Scheme 1. Cascade reaction of pyridine with DMAD

The nucleophilicity of N-1 in imidazo[1,2-*a*]pyridine is expected to be further substantiated by the lone-pair of the pyridine-ring nitrogen atom. In view of this, we perceived the imidazo[1,2-*a*]pyridine molecule to be a suitable precursor for the generation of a 1,4-dipole from its reaction with DMAD. Upon looking into the literature, it was found that Cossio and co-workers carried out the reaction of substituted imidazo[1,2-*a*]pyridines with benzyne, generated *in situ* from 2-(trimethylsilyl)phenyl trifluoromethylsulphonate, in which [8+2] cycloaddition occurred; however, no reaction of imidazo[1,2-*a*]pyridine with DMAD was reported.[11] Upon carrying out the reaction of imidazo[1,2-*a*]pyridine with DMAD, we succeeded in obtaining the first representative of CCMB isoconjugate with the odd non-alternant hydrocarbon anion (Scheme 2).[12]

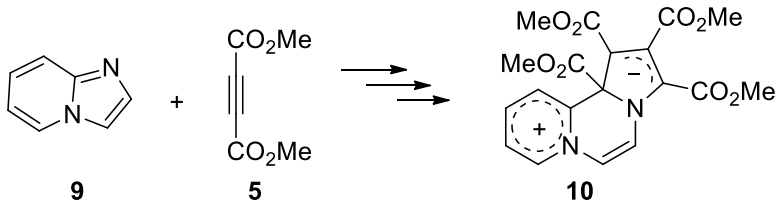

Scheme 2. Formation of a CCMB from the reaction of imidazo[1,2-*a*]pyridine with DMAD.

The CCMBs are known to exhibit remarkable material properties and, thus, have garnered much attention in the field of materials chemistry for the development of new switchable materials with high data-storage capacity.[13] They bind with a polymer to give film coatingswhich are quite stable and easy to handle and, therefore, have been a point of interest for the researchers to develop such polymerizable mesoionic scaffolds.[14] This has been backed up by constant efforts to develop new synthetic protocols to enlarge the libraries of these structural motifs.[15]

Furthermore, azaindolizines have received a great deal of attention in the last few decades owing to their bioactivity. There is a plethora of such compounds that are anti-microbial, anti-bacterial and anti-fungal in nature.[16] Since these compounds are multifunctional, it seemed plausible to explore the possibilities of

synthesizing CCMBs, which not only work as potential materials, but may also be bioactive. In order to synthesize such pharmaceutically interesting betaines, annulated pyridines were found to be a good starting material since they are a part of many medicinally active compounds.[17]

Like DMAD,[18] maleic anhydride[19] has also been found to be a versatile tool in organic synthesis due to the presence of an electron-deficient C=C functionality conjugated with a cyclic anhydride structure. For example, Cookson et al. reported the reaction of pyridazine with maleic anhydride to give an *exo* type cyclic 1:2-adduct (**11**) which was not polymeric in nature (Figure 2).[20] This motivated us to investigate the reaction of imidazo[1,2-*a*]pyridines with maleic anhydride which led to the synthesis of new CCMBS. In addition, the synthesized products display intramolecular charge-transfer phenomena, which enhances the possibility of their use as luminescent materials. The results are presented herein.

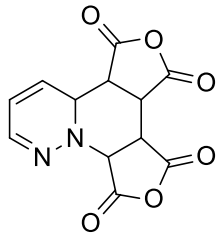

11

Figure 2. 1:2-Adduct of pyridazine with maleic anhydride.

Results and Discussion

Maleic anhydride (**13**) (2 equiv.) reacted with imidazo[1,2-*a*]pyridines (**12a-d**) in acetonitrile at room temperature (r.t. ~ 35 °C) to afford compounds **16** and **15b-d** as brown solids (Scheme 3).

The reaction of imidazo[1,2-*a*]pyridine with maleic anhydride proceeded almost similarly to its reaction with DMAD[12], i.e., the reaction generates a 1,4-dipole (**14**) which subsequently reacts with a second molecule of maleic anhydride to form **15.** Nevertheless, there are some distinct differences between the two reactions. In contrast to the reaction with DMAD, in the present case, the zwitter ion **15** does not cyclize at C-9, nor does a 1,5-alkyl shift take place. The non-occurrence of these two structural changes with maleic anhydride can be attributed to the absence of a conjugated -HC=CH-CH=CH- system between C-10 and C-16.

Unexpectedly, it was found that the further course of the reaction is determined by the nature of R at the 2-position. In the case of R = H, i.e., the 2-position being unsubstituted, the initially formed product, **15**, undergoes a 1,3-H shift to give **16** as the final product. When R = Ph or *p*-substituted phenyl group, no further change takes place. As described later, both products have been duly characterized. We do not have any plausible explanation for this difference in their behaviors, however, as discussed
later, the activation free energy barrier ($\Delta G^{\#}$) for a 1,3-H shift in the case of **15b** substituted by the phenyl group at the 2-position is greater than that for the unsubstituted **15** by 4 kcal mol^{-1}. Thus, the differences in the behavior of **15b-d** may be attributed to steric hindrance caused by the phenyl group.

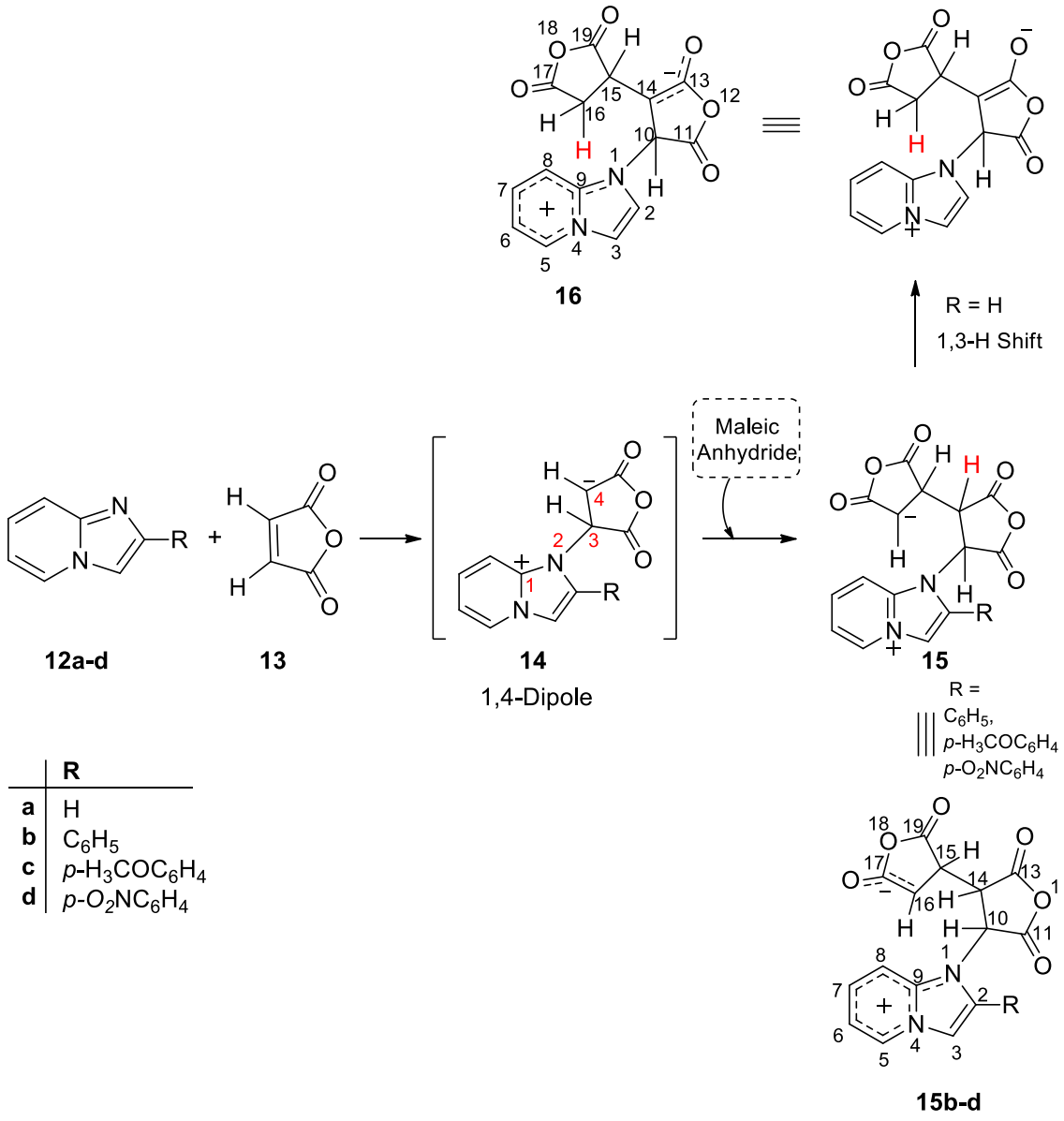

	R
a	H
b	C_6H_5
c	*p*-$H_3COC_6H_4$
d	*p*-$O_2NC_6H_4$

Scheme 3. Reactions of imidazo[1,2-*a*]pyridines with maleic anhydride.

Although our repeated attempts to grow a single crystal were unsuccessful, the structures of the products **16** and **15b-d** could be established unambiguously based on extensive spectral studies. The ^{1}H NMR spectrum of **16** is reproduced in Figure 3.

The most characteristic feature of the spectrum is the presence of three protons, H_A, H_B and H_C, constituting an ABC spin system to give three sets of doublets of doublets (dd). Thus, three dds at δ 3.30 (dd, $^2J_{HH}$ 17.2 Hz, $^3J_{HH}$ 9.6 Hz), 3.44 (dd, $^2J_{HH}$ 17.2 Hz, $^3J_{HH}$ 4.8 Hz) and 5.69 (dd, $^3J_{HH}$ 9.6 Hz, $^3J_{HH}$ 4.8 Hz) could be assigned to the protons C-16H_A, C-16H_B and C-15H_C, respectively. This structural feature is further corroborated by studying its ^{13}C NMR spectrum in conjunction with its ^{13}C DEPT 135 NMR spectrum reproduced in Figure 4.

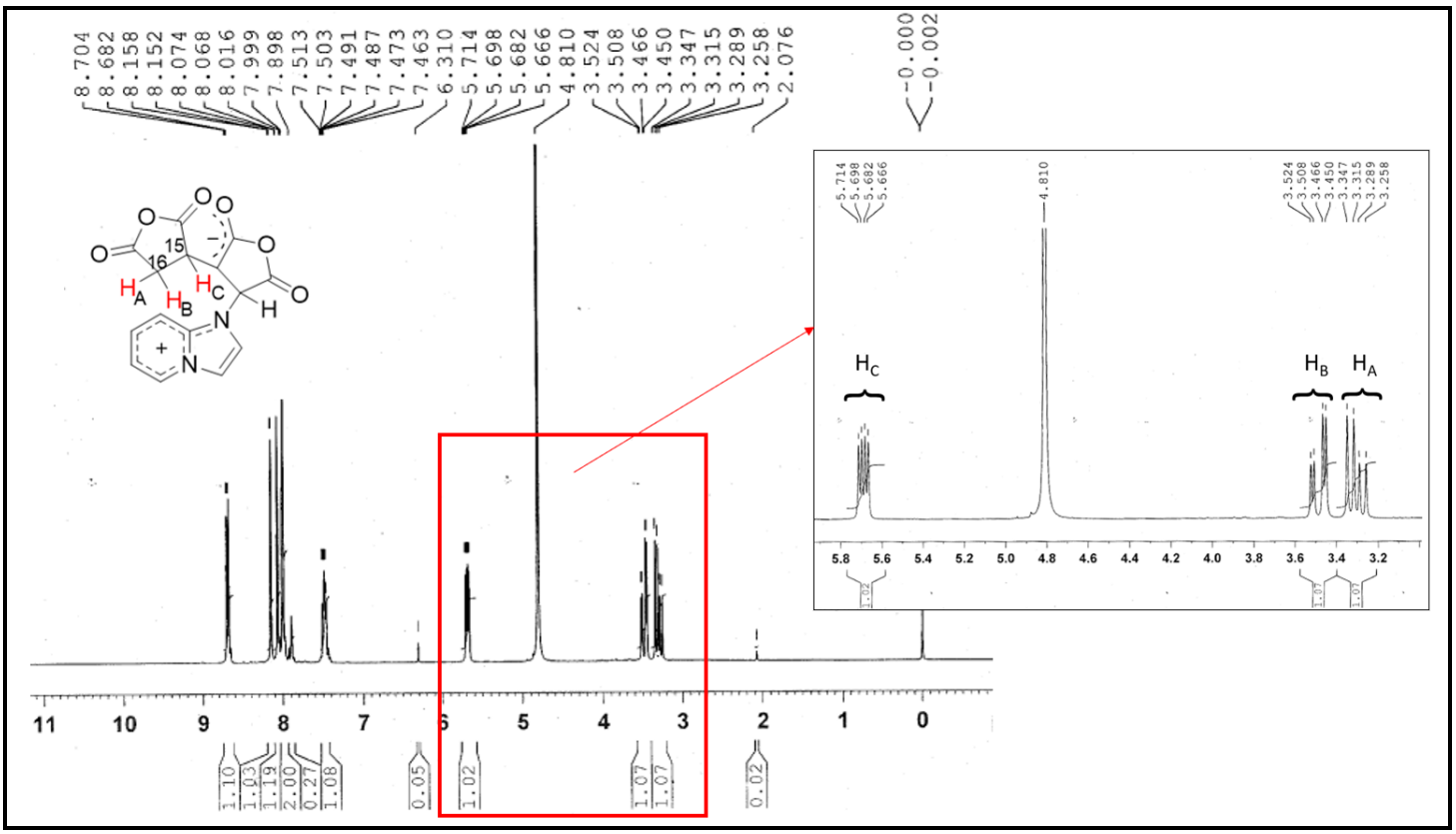

Figure 3. ^{1}H NMR spectrum of the product **16** depicting the ABC spin system.

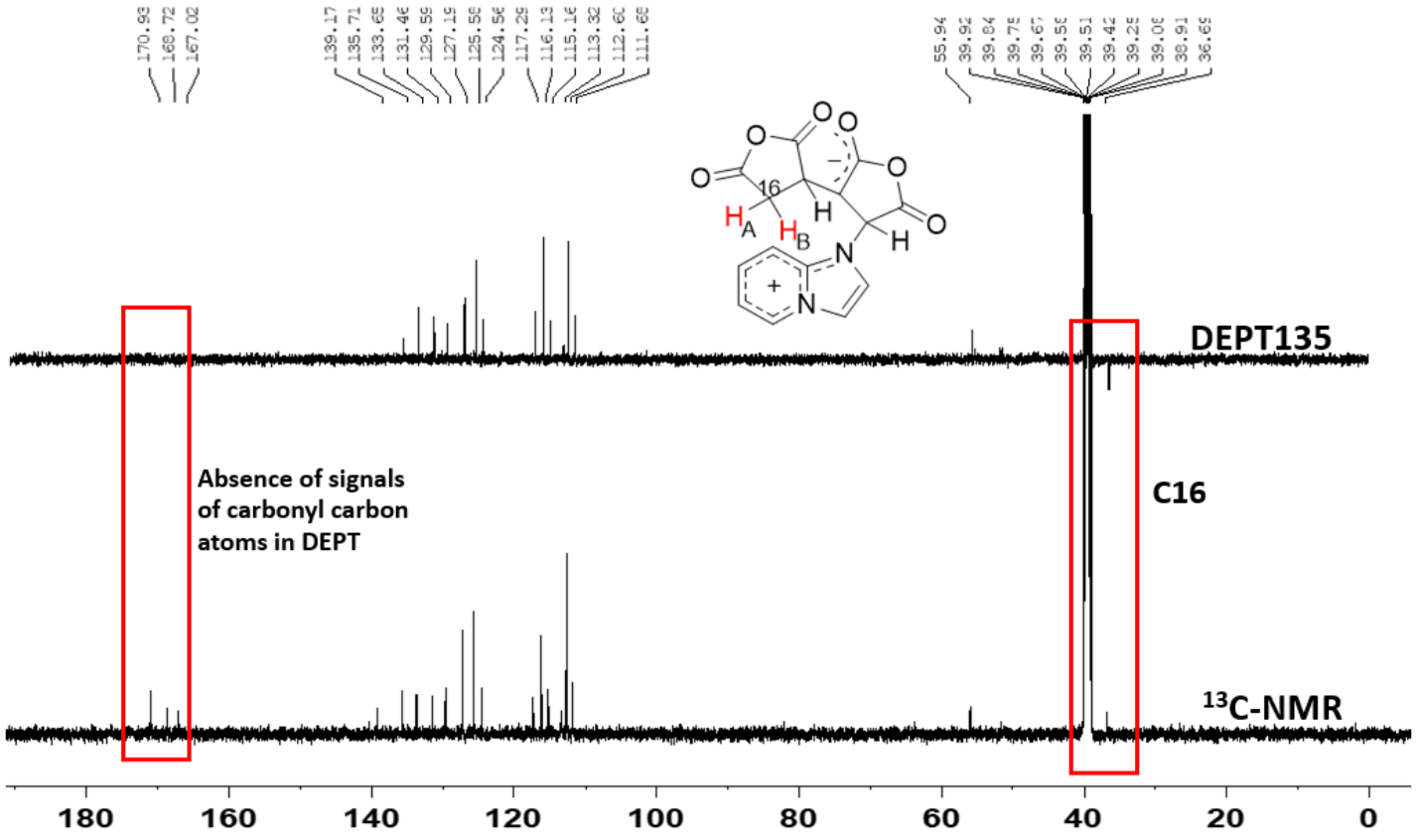

Figure 4. ^{13}C NMR spectrum of **16** and its DEPT 135 version.

It is noteworthy that a ^{13}C NMR signal at δ 36.7 is reverted in the DEPT135 spectrum, confirming the presence of a CH_2 moiety. Furthermore, the presence of only three carbonyl groups is confirmed by three ^{13}C NMR signals in the downfield region of δ160 – 171 ppm which disappear in the DEPT spectrum. The absence of the enolic hydrogen atoms is further confirmed by the deuterium-exchange experiment in which no change was observed. The presence of the ABC spin system is confirmed by 2D-NMR spectra, namely the COSY and HMQC spectra. In the COSY spectrum, reproduced in the Supplementary Material (SM) (S4), correlation contours can be seen between the ^{1}HNMR signals of the protons H_A and H_B on one side and H_C on the other side. Furthermore, in the HMQC spectrum of the same compound (reproduced in SM-S4), correlation contours can be noted between the ^1H NMR signals of the protons H_A and H_B on the X axis with the ^{13}C NMR signal of C-16 on the Y axis, and, similarly, between the ^1H NMR signal of the proton H_C on the X axis with the ^{13}C NMR signal of C-15 on the Y axis.

Contrary to this NMR data, no ABC spin system could be found in the ^1H NMR spectrum of **15b** (reproduced in SM). Instead, two partially resolved doublets, at δ 4.21 ($^3J_{HH}$ 8.8 Hz) and δ 3.67 (unresolved), and two partially resolved triplets at δ 4.04 ($^3J_{HH}$ 9.0 Hz) and δ 3.82 (unresolved) could be assigned to the protons H-10, H-16, H-14 and H-15, respectively. Furthermore, in the ^{13}C NMR and ^{13}C-DEPT135 experiments (reproduced in SM), no inverted peak for the CH_2 group was observed, although the presence of three carbonyl groups could be substantiated.

Analogously, in **15c** and **15d**, similar peaks are expected to appear in the range of δ 3-4 ppm which apparently merged with the DMSO peak in their ^{1}H-NMR (See SM).

In addition, $[M+H]^+$ peaks of **16,** and **15b-d**, obtained at 315.2570, 391.3456, 421.3771, 437.0878, respectively, are in agreement with the molecular weights of the proposed structures.

In the absence of X-ray crystal-structure analysis, it was not possible to determine the absolute configuration of any product. As discussed above, however, the two protons of the CH_2 moiety in the product **16** are diastereotopic, constituting an ABC spin system with vicinal proton Hc. This indicates the presence of chirality in the molecule, which is confirmed by the optical activity measured for the compound **16** ($[\alpha]_D^{25^\circ}$ = -286.39°). As discussed later, the theoretical investigation and optimization of the geometry of **16** reveals the presence of an axis of chirality in these compounds.

Molecular electrostatic potential maps

The molecular electrostatic potential (MEP) maps visualized using GaussView 6 depict the distribution of electron densities in different regions of a molecule.[21] The regions of the highest and least electron densities in the molecule are portrayed by the red and blue colours, respectively, and the electron densities decrease in the order red > orange > yellow > green > blue. Thus, on the basis of the colours in the MEP, it is possible to predict, qualitatively, the nucleophilic and electrophilic sites in the molecule.[22,23] The MEP maps of the CCMBs **16** and **15b-d** are shown in Figure 5.

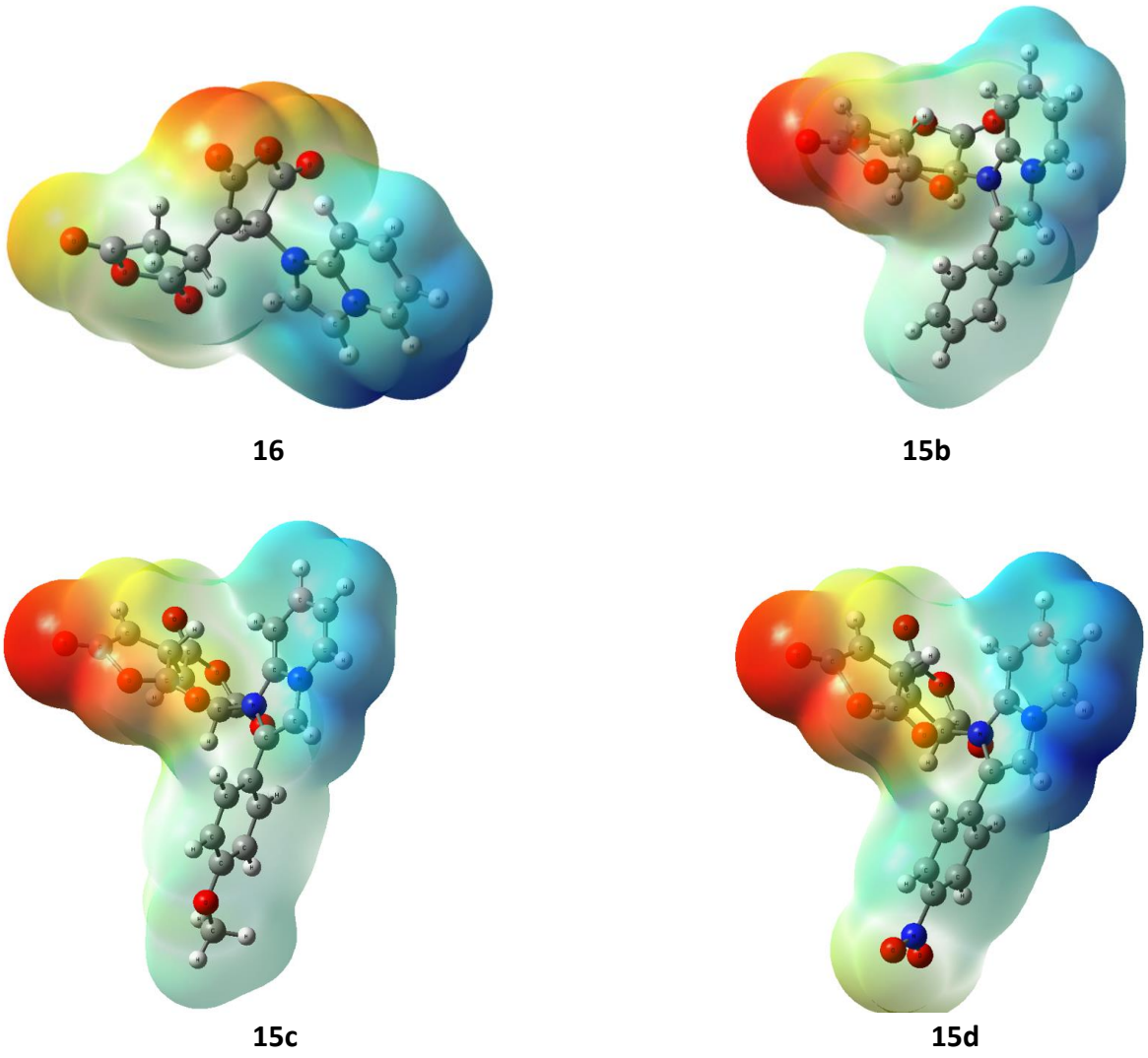

Figure 5. Molecular electrostatic maps of the CCMBs **16, 15b-d.**

It may be noted that the blue colour is concentrated on the imidazolopyridinium part of the molecules, indicating its electron-deficient character, whereas the red colour is spread over the maleic anhydride part, revealing its electron-rich nature. This feature is evident in the frontier molecular orbitals (FMOs) which is also explained later. Furthermore, in the case of **15b-d**, having a phenyl or *p*-substituted phenyl substituent group at the 2-position of imidazo[1,2-*a*]pyridine, the densities of the blue and red colours are further enhanced, revealing their increased electrophilic and nucleophilic characters, respectively. This aspect is reflected in a bathochromic shift in the UV-Vis absorption band in these cases, which is discussed later.

Frontier molecular orbitals and charge transfer phenomena

The location and separation of the FMOs are other characteristics of the CCMBs.[2,24] The HOMO and LUMO of the product **16** are shown in Figure 6.

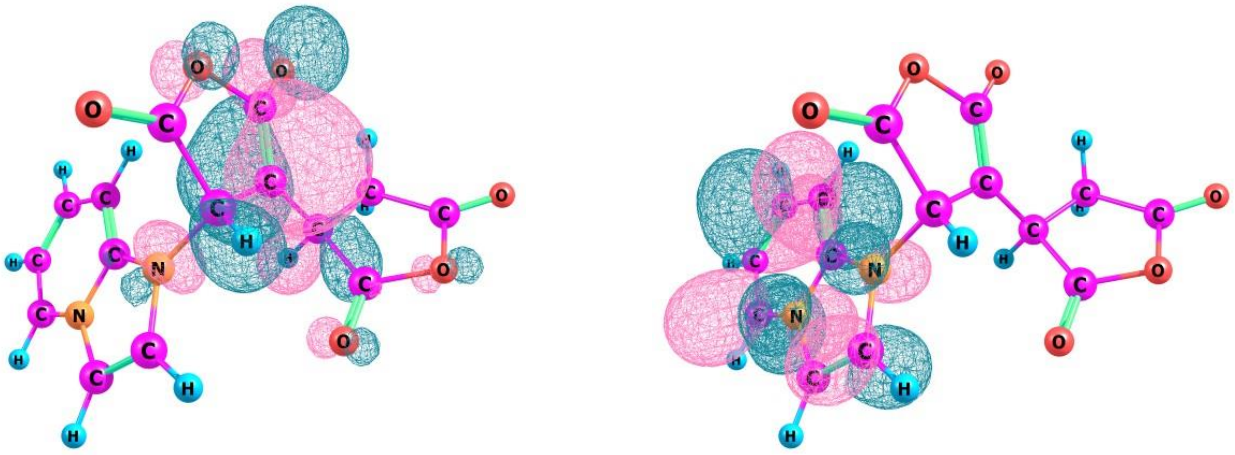

HOMO
E = - 0.1999 eV

LUMO
E = -0.1093 eV

Figure 6. Kohn-Sham HOMO and LUMO of **16.**

It is noteworthy that, in accordance with the MEP maps described earlier, the HOMO is centered on the maleic anhydride part of the molecule, whereas the LUMO is located on the imidazopyridine part. Furthermore, these two parts face each other. This structural feature makes effective intramolecular charge transfer (ICT) possible, which is an important physical phenomenon present in the molecules having both electron-donating (D) and electron-accepting (A) substituent groups or regions.[25] The ICT was found to be accompanied by twisting of the conformation, defined as twisted intramolecular charge transfer, abbreviated as TICT.[26] Energies of the FMOs of the four CCMBs **16** and **15b-d** are presented in Table 1.

Table 1. Energies of the FMOs of the CCMBs **16** and **15b-d**

Entry	HOMO (eV)	LUMO (eV)	$E_{LUMO-HOMO}$ (kcal mol^{-1})
16	-0.1999	-0.1093	2.09
15b	-0.1641	-0.1085	1.28
15c	-0.1596	-0.1135	1.06
15d	-0.1726	-0.1307	0.97

Interestingly, the energy gap between HOMO and LUMO of **16** is only 2.09 kcal mol^{-1}, which further decreases on substitution at the 2-position by the phenyl or substituted phenyl group. In **15d**, it is reduced to 0.97 kcal mol^{-1} only (Figure 7) causing a bathochromic shift in the UV-Vis absorption which is discussed later.

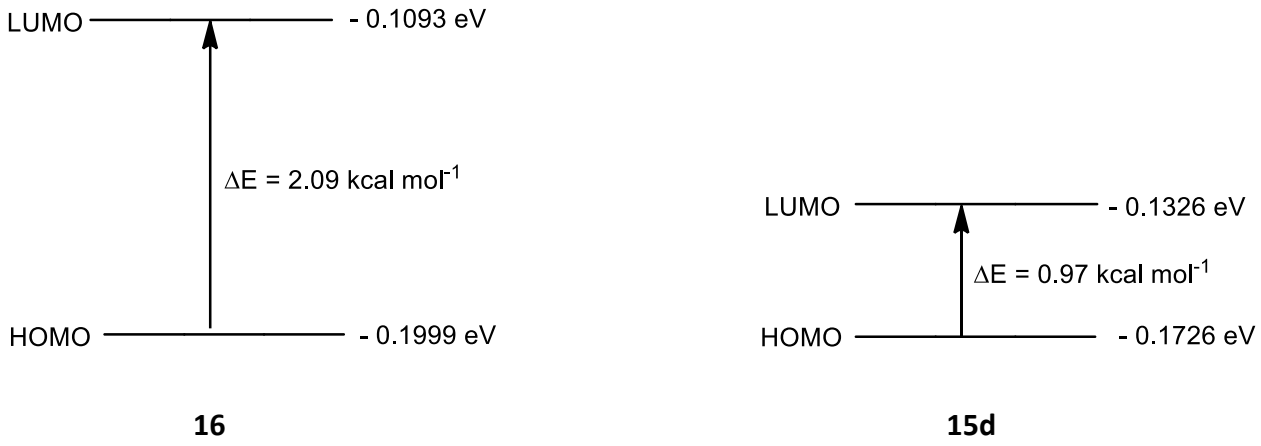

Figure 7. The HOMO-LUMO energy gaps in **16** and **15d.**

Dipole moment and conductivity measurements

Dipole moment and electrical conductivity are important criteria of the molecules involved in charge transfer.[27] Yates and co-workers determined dipole moments of *p*-(N,N-dimethylamino)benzonitrile systems in the ground and excited states, and change in the excited state was attributed to twisting of the conformation.[28] We computed the dipole moments in the ground and excited states of the four compounds at the wB97xd/6-311++G(d,p) level. The three axes in CCMB **16** are shown in Figure 8.

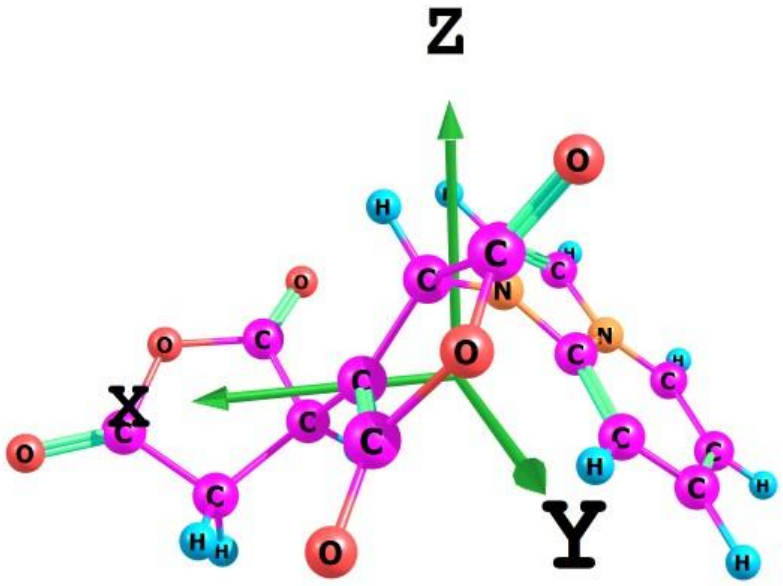

Figure 8. The three axes of the dipole moment of **16** computed at the wB97xd/6-311+G(d,p) level.

The three components and total values of the dipole moments in the ground and excited states of **16** and **15b-d**, computed at the wB97xd/6-311+G(d,p) level, are shown in Table 2.

Table 2. Dipole moments of CCMB **16** and **15b-d** computed at the wB97xd/6-311+G(d,p) level.

Entry	Ground State				Excited State			
	X- axis	Y- axis	Z- axis	Total (Debye)	X- axis	Y- axis	Z- axis	Total (Debye)
16	12.8181	-7.1183	4.5861	**15.36**	0.6524	-3.6045	-2.2565	**4.30**
15b	-11.3252	11.7064	1.8755	**16.40**	-2.1966	-2.9362	0.2084	**3.67**
15c	4.7320	-15.8224	0.2278	**16.52**	2.1484	2.0555	1.0967	**3.17**
15d	-2.5742	-16.7642	-1.9401	**17.07**	-5.1920	0.7490	-0.6630	**5.29**

It may be noted that dipole moments of all of the compounds in the ground state are high. Substitution at the 2-position by the phenyl or the *p*-substituted phenyl group is accompanied by an increase in the dipole moment, this effect being expectedly maximized in the case of **15d** having the *p*-nitrophenyl group. In the excited state, values of the dipole moments decrease in all the cases, which may be attributed to distortion of the conformations.

Electrical conductivity is an important criterion for classifying organic molecules as conductors, semi-conductors and insulators.[29-32] Zobel *et* al. studied the dependence of electrical conductivity of some CT complexes containing 7,7,8,8-tetracyano-*p*-quinodimethane (TCNQ) as an acceptor on temperature. A fast and monotonic decrease of conductivity with decreasing temperature was detected, which is a characteristic property of a regular semiconductor. Furthermore, on plotting ln[*I*] against 1/T (in Kelvin) at constant voltage, a straight line was obtained.[32]

We, therefore, determined the molar conductance of the four compounds at varying temperatures; the results are presented in Table 3.

Table 3. Variations of molar conductance of **16** and **15b-d** with temperature in 10^{-3}M DMSO.

Entry	Specific Conductance at ~30°C ($\Omega^{-1}cm^2$)	Molar Conductance I ($\Omega^{-1}cm^2mol^{-1}$)					
		10°C	20°C	30°C	40°C	50°C	60°C
16	12.30 x 10^{-6}	4.60	11.20	12.30	19.30	25.40	30.50
15b	18.40 x 10^{-6}	7.70	11.90	18.40	23.10	27.70	34.20
15c	26.10 x 10^{-6}	16.10	18.20	26.10	31.90	38.80	46.50
15d	06.40 x 10^{-6}	2.30	5.10	06.40	09.70	13.80	19.40

The graphs between ln[*I*] and 1/T (K) for the four compounds are shown in Figure 9.

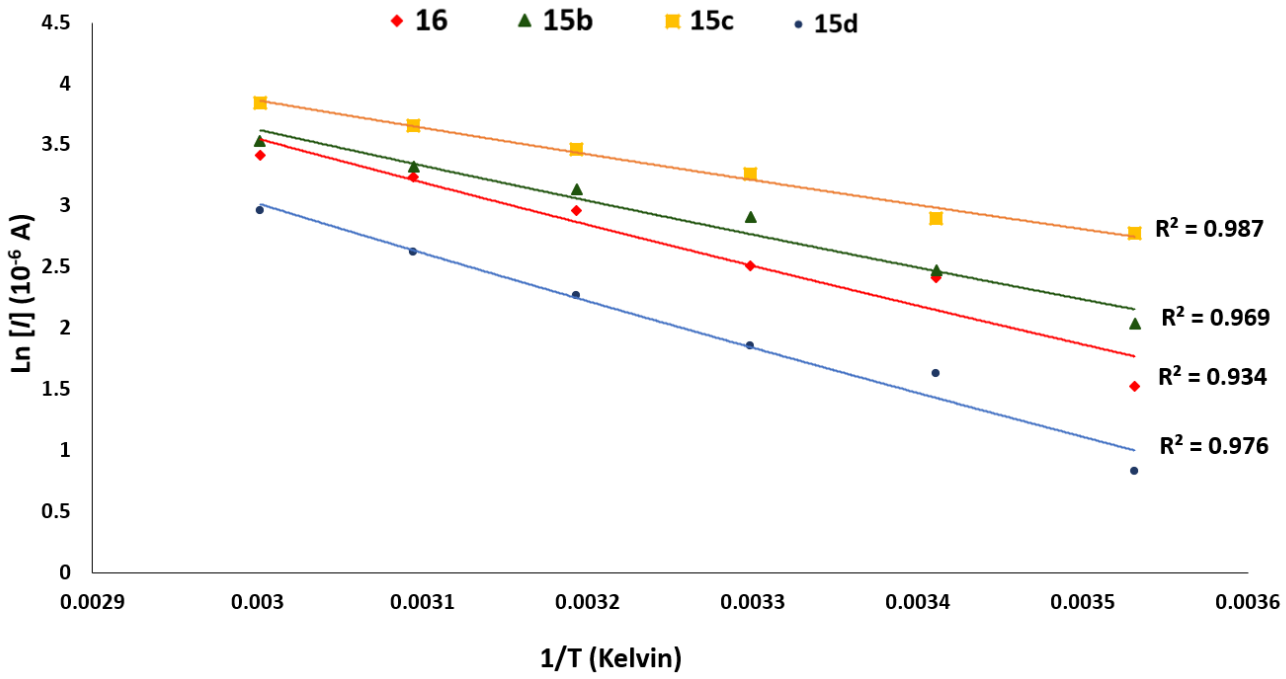

Figure 9. Temperature dependence of the molar conductivity of **16** and **15b-d**.

It is evident that all four compounds are electrically conducting; it is interesting to find that, in accordance with the earlier results, molar conductivity decreases with decreasing temperature. The fast and monotonic decrease of conductivity with decreasing temperature reveals regular semiconducting character needing thermal activation for the electrons and holes. The conductivity is small at low temperatures which is caused by lack of carriers. This monotonic decrease is also a strong hint that no phase transition occurs, at least between room temperature and ~200 K. Furthermore, specific conductance of **15c**, having the electron-releasing OMe group is highest, whereas that of **15d**, having the electron-withdrawing NO_2 group, is smallest.

Fluorescence spectroscopy

Fluorescence spectroscopy has been extensively employed for investigating the excitation and emission behavior of the molecules such as *p*-(N,N-dimethylamino)benzonitrile and related substances, involving intramolecular charge transfer.[33-37] The fluorescence emission spectrum is accompanied by a red shift, the magnitude of which is influenced by solvent, concentration, temperature and environment, i.e., the nature of the substituent groups. The fluorescence spectra of the compounds **16**, and **15b,c** are shown in Figure 10. The compound **15d** did not fluoresce (discussed later).

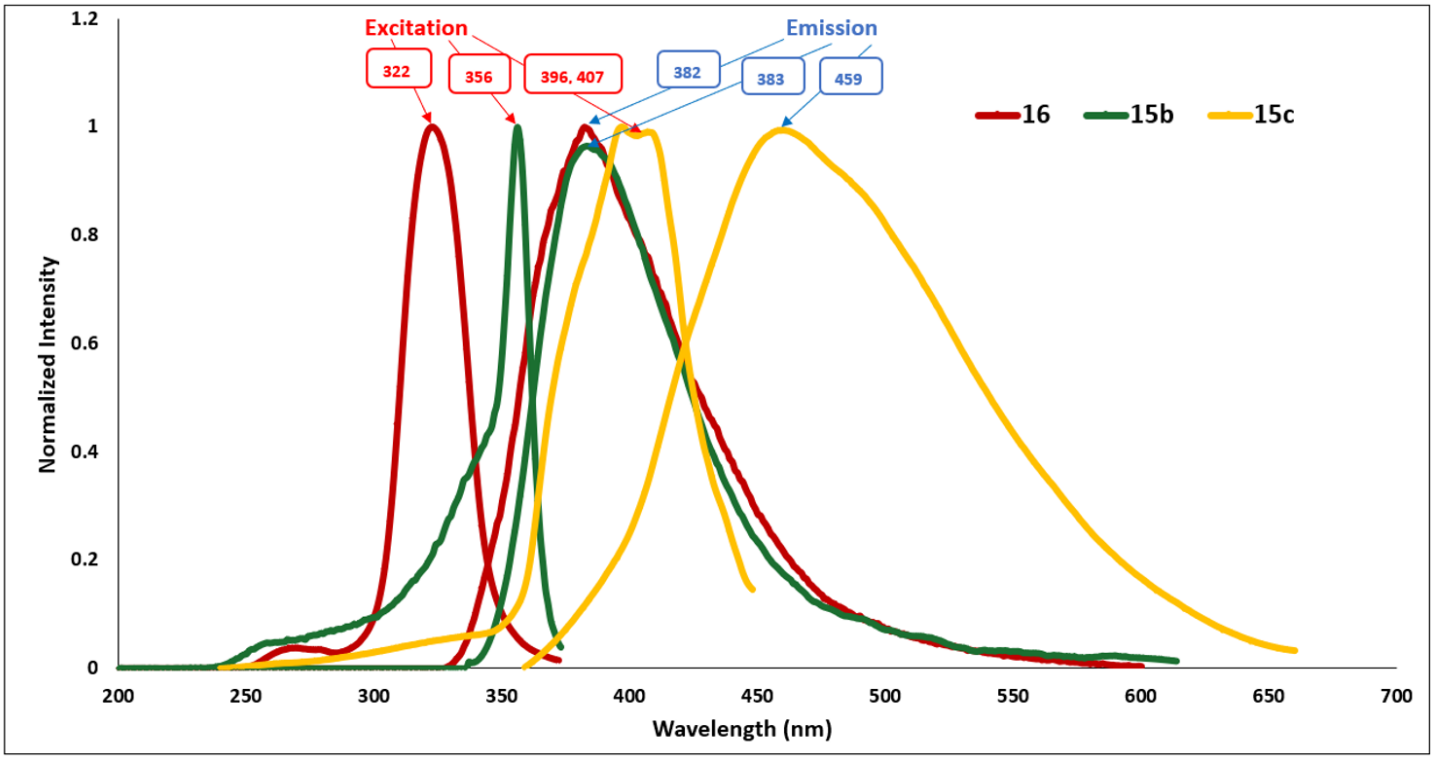

Figure 10. The fluorescence excitation and emission spectra of the compounds **16**, and **15b,c** in DMSO at room temperature.

Several characteristic features are noteworthy. The excitation and emission spectra are almost mirror images, confirming it to be a 0-0 transition ($S_1 \rightarrow S_0$). The emission is accompanied by a red shift, ranging from 27 to 63 nm. The magnitude of the red shift is highest in the case of **15c** which has an electron-releasing OMe group. Moreover, in this case, excitation is detected at two wavelengths, 396 and 407 nm. As mentioned earlier, fluorescence could not be detected in the case of **15d** which has a nitro group. It has been reported that, occasionally, a strong EWG such as a nitro group acts as quencher and the compound does not fluoresce.[38]

Spectrophotometric studies and time-dependent DFT calculations

Spectrometric methods have been widely used for studying the CT complexes.[39,40] In view of this, we investigated the intramolecular CT phenomenon in **16,** and **15b-d** with UV-Vis spectroscopy. The curves obtained are shown in Figure 11.

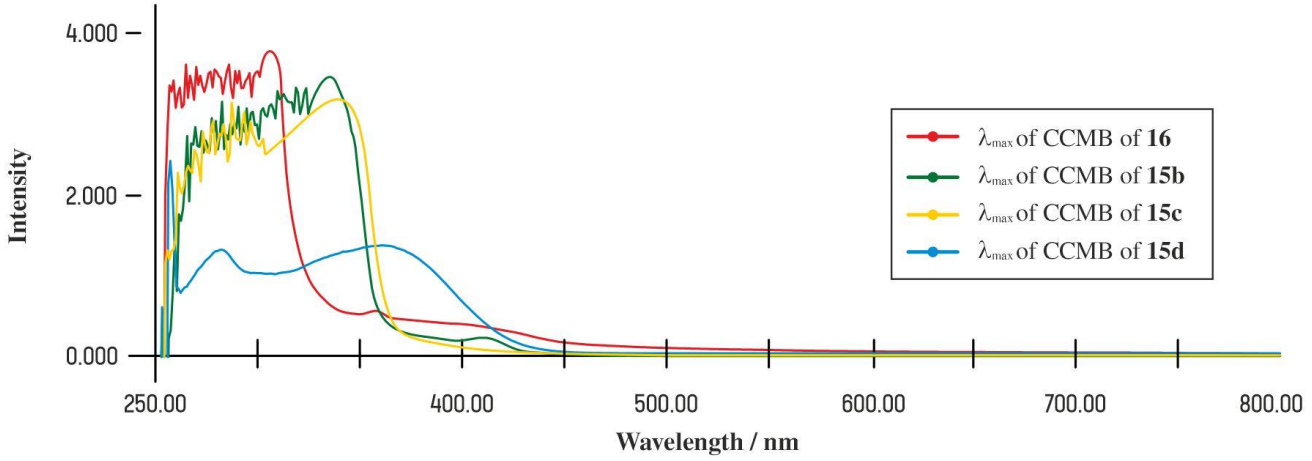

Figure 11. The electronic spectra of **16,** and **15b-d** in DMSO.

A shoulder observed in the range of 280-320 nm can be assigned to the intramolecular CT complex. It is noteworthy that the *λmax* corresponding to CT excitation is very close to that observed in the fluorescence spectra.

In recent years, time-dependent density-functional theory (TDDFT) calculations have been employed extensively for studying properties of the electronically excited states (EES).[39] With the help of TDDFT, various properties of the EES, such as the amount of the charge transfer, and changes in the geometric parameters resulting from the photon absorption by the CT complexes, could be determined successfully.[41,42]

We carried out TDDFT calculations of the CCMBs **16,** and **15b-d** at the wB97XD/6-311+G(d,p) level. The experimental and theoretically calculated values of the λmax are presented in Table 4.

Table 4. Experimental and theoretically-calculated values of the λmax of **16** and **15b-d.**

Entry	***λmax* (nm)**	
	Theoretical value of CT	**Experimental value**
16	263 nm	361 nm, 307 nm
15b	339 nm	335 nm, 317 nm
15c	302 nm	339 nm, 288 nm
15d	347 nm	359 nm, 281 nm

It may be noted that, except in the case of **16**, theoretically calculated values of the *λmax* are shifted to longer wavelengths as compared to the experimentally-determined values. It has been reported earlier that TDDFT calculations underestimate CT excitation energies.[43]

Theoretical investigation of the model reaction sequence

We investigated the following sequence of model reactions theoretically at the B3LYP/6-31+G(d) level using the Gaussian 16 suite of programs.[44] (Scheme 4).

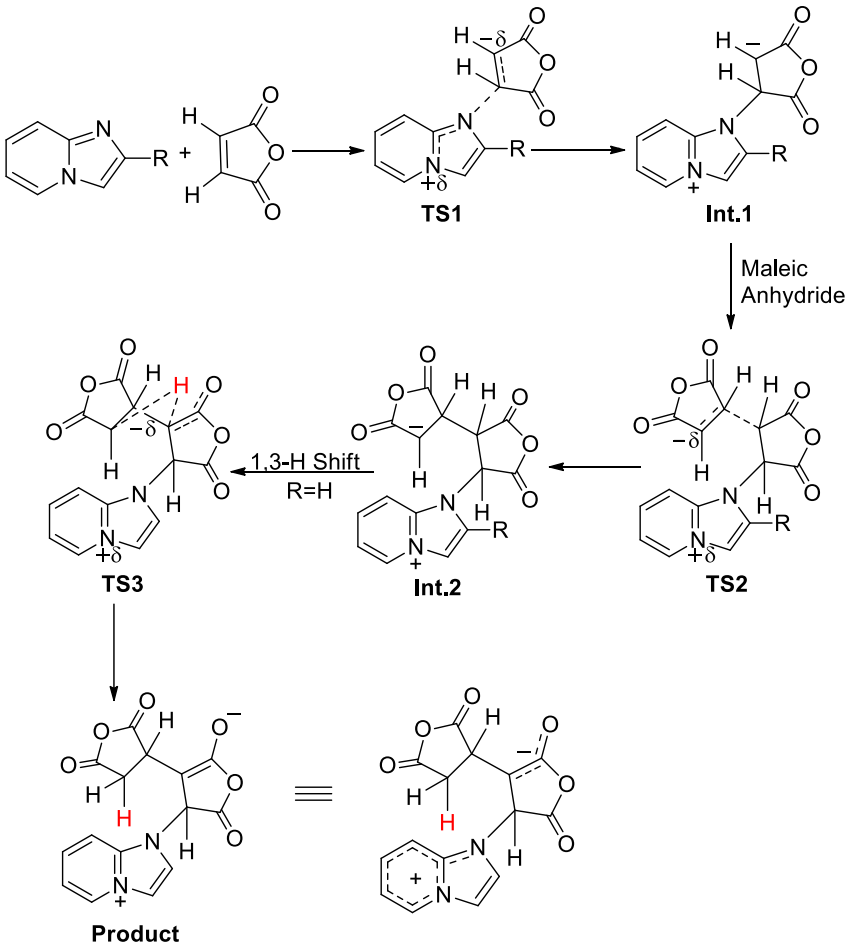

Scheme 4. Model reaction of imidazo[1,2-*a*]pyridine with maleic anhydride computed at the B3LYP/6-31+G(d) level in gas phase.

The optimized geometries of all the species involved in the reaction of imidazo[1,2-*a*]pyridine with maleic anhydride are shown in Figure 12.

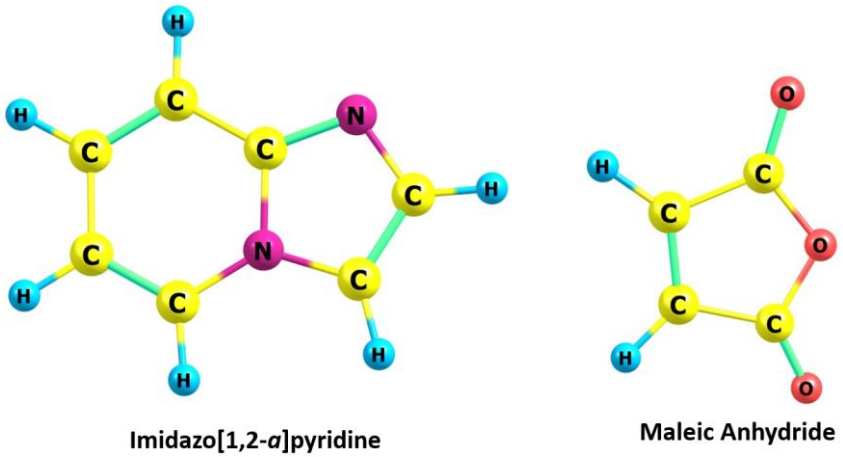

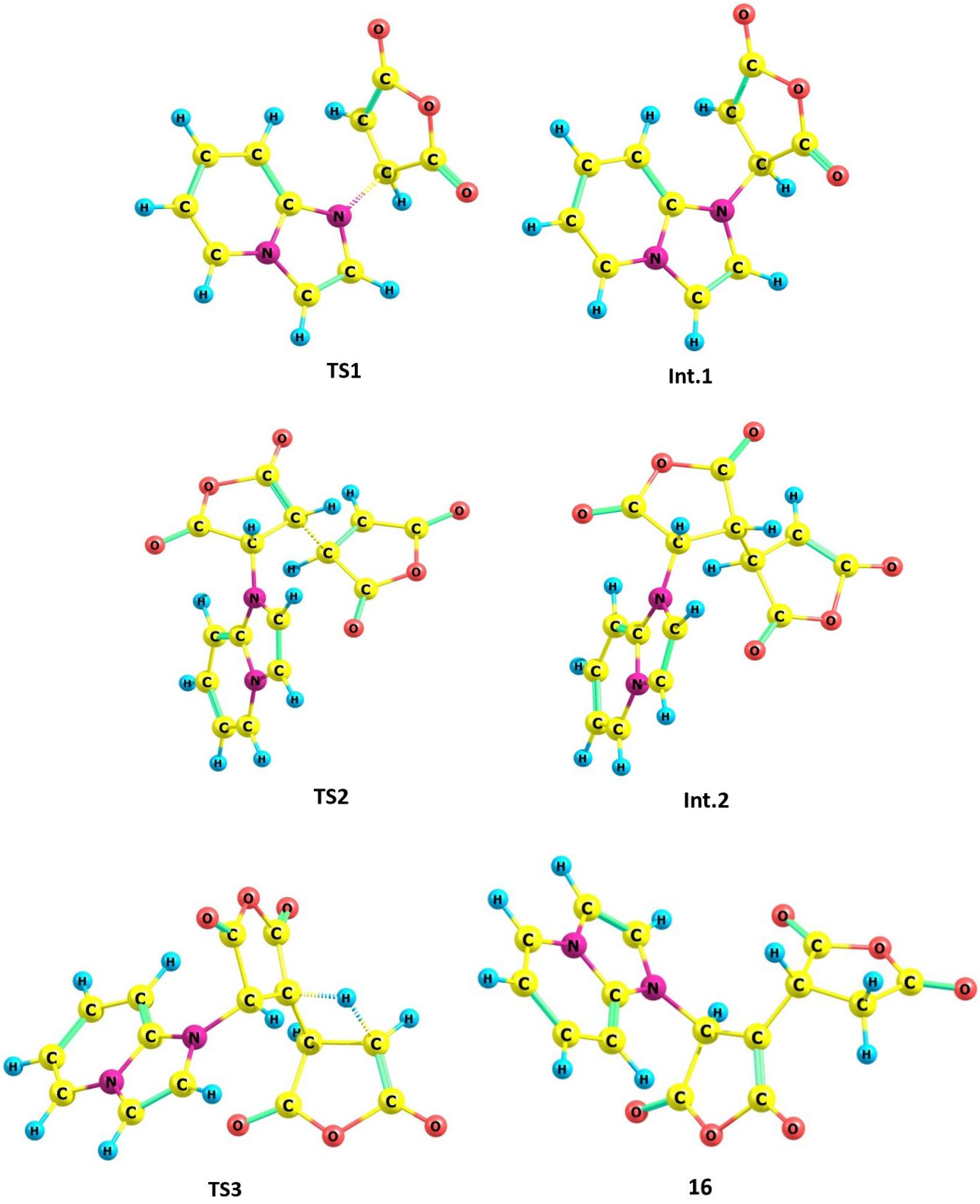

Figure 12. The geometries of different species involved in the reaction of imidazo[1,2-*a*]pyridine with maleic anhydride optimized at the B3LYP/6-31+G(d) level.

As discussed earlier, in the absence of X-ray crystal structure analysis, absolute configuration could not be ascertained; however, an axis of chirality can be seen in the optimized geometry of the product **16 (**Figure 13).

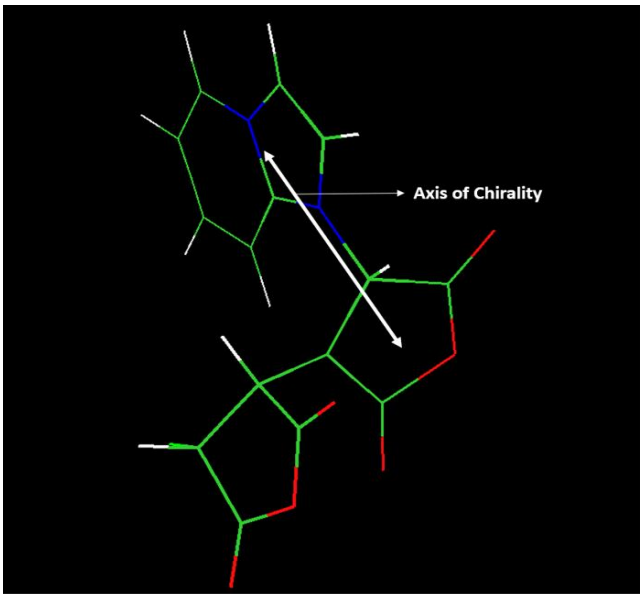

Figure 13. Axis of chirality in **16** optimized at the B3LYP/6-31+G(d) level.

The thermodynamic data of the reactions of imidazo[1,2-a]pyridines **12a,b** with maleic anhydride are presented in Table 5.

Table 5. Thermodynamic data of the formation of **16** and **15b** computed at the B3LYP/6-31+G(d) level.

Reaction		12a + 2 equiv. Maleic Anhydride	12b + 2 equiv. Maleic Anhydride
Step 1 (Formation of 1,4-Dipole)	**$\Delta H^{\#}$**	20.35	17.31
	$\Delta G^{\#}$	32.48	28.95
	ΔH^{o}	21.32	17.31
	ΔG^{o}	33.14	28.94
Step 2 (Attack of 1,4-Dipole on 2nd molecule of E^{+})	**$\Delta H^{\#}$**	5.21	9.21
	$\Delta G^{\#}$	**18.79**	**21.81**
	ΔH^{o}	31.12	23.59
	ΔG^{o}	56.93	47.70
Step 3 (1,3-H shift)	**$\Delta H^{\#}$**	13.00	15.87
	$\Delta G^{\#}$	12.66	16.41
	ΔH^{o}	1.67	-3.55
	ΔG^{o}	26.27	20.19

$\Delta H^{\#}$, ΔH^{o}, $\Delta G^{\#}$ and ΔG^{o} are in kcal mol^{-1}

The free energy profiles of the whole sequence of reactions between imidazo[1,2-*a*]pyridine and maleic anhydride are depicted in Figure 14.

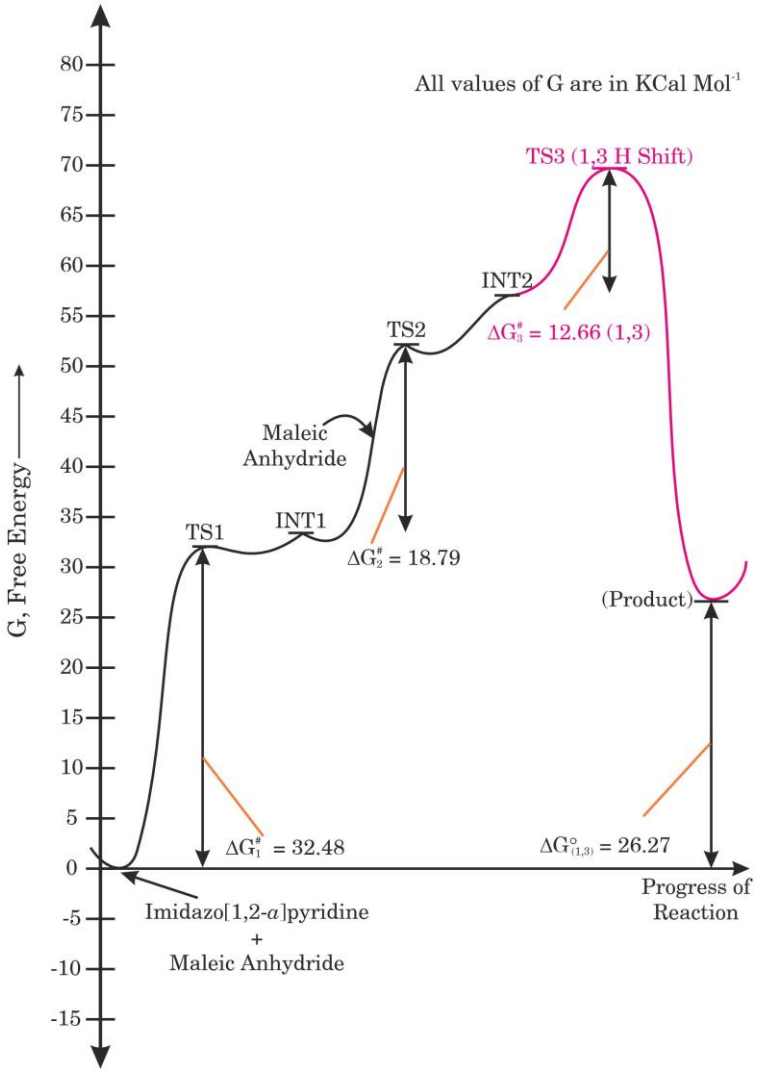

Figure 14. Free-energy profile of the reaction of imidazo[1,2-*a*]pyridine with 2 equiv. maleic anhydride computed at B3LYP/6-31+G(d) level.

The overall reaction is completed in three steps. The first step, having a high-activation free-energy barrier ($\Delta G^{\#}$ = 32.48 kcal mol^{-1}), is the rate-determining step. The reaction is endergonic (ΔG° = 26.27 kcal mol^{-1}) which explains why the present reaction is much slower than the reaction of imidazo[1,2-*a*]pyridine with DMAD.[8] From these data, it might be concluded that completion of reaction requires heating, however, it is not needed, possibly due to comparatively high ambient temperature (~ 30 °C). Furthermore, the last step involving a 1,3-H shift has an activation barrier of $\Delta G^{\#}$ = 12.66 kcal mol^{-1}, but the resulting species has the negative charge delocalized over a larger area which appears to be the driving force. As mentioned earlier, in the reaction of 2-phenyl- (or *p*-substituted phenyl) imidazo[1,2-*a*]pyridine with maleic anhydride, a 1,3-H shift does not take place. In view of this, we investigated the reaction of 2-phenyl- imidazo[1,2-*a*]pyridine with maleic anhydride. Theoretical and thermodynamic data are presented in Table 1. It may be noted that, although the activation free energy barrier ($\Delta G^{\#}$) for the first step is lower than that for the reaction of unsubstituted imidazo[1,2-*a*]pyridine, the activation free energy barriers for the second and third steps are

higher by *ca.* 3 and 4 kcal mol^{-1}, respectively. This may be the reason why a 1,3-H shift does not take place in the reaction of 2-substituted imidazo[1,2-*a*]pyridines.

Conclusions

The reactions of imidazo[1,2-*a*]pyridines with maleic anhydride afford new CCMBs. Physico-chemical studies, including dipole moments, electrical conductivity, fluorescence spectroscopy and UV-Vis spectroscopy reveal the existence of intramolecular charge-transfer phenomena and the luminescent character of these compounds. A theoretical investigation of the model reaction of imidazo[1,2-*a*]pyridine with maleic anhydride helps to rationalize whole sequences of reactions. MEP maps and FMOs show that negative and positive charges are restricted to two different parts of the molecule, in accordance with the characteristic structural feature of the CCMBs, and they face each other. The latter geometrical feature facilitates active intramolecular charge transfer and induces luminescent character in these compounds.

Experimental Section

General.. Commercially available imidazo[1,2-a]pyridine (**12a**) procured from Merck was directly used for the synthesis. Maleic anhydride was purified by sublimation prior to setting up the reaction. Solvents such as THF and acetonitrile were freshly dried and distilled according to known procedures. Melting points were measured in an open capillary and are reported as such without any correction. The UV-visible spectra were recorded on a Shimadzu 160 UV-vis spectrophotometer in the range of 200–800 nm with a quartz cell of 1-cm path length. The IR spectra were recorded on a Bruker FT IR spectrometer ALPHA II using KBr pellet. The wavenumbers (ν_{max}) of the recorded IR signals are reported in cm^{-1}. The ^{1}H NMR spectra were obtained at 25°C on a Jeol Resonance ECS 400 MHz NMR spectrometer and Bruker-DPX-300 MHz spectrometer while ^{13}C NMR, DEPT 135, COSY and HMQC spectra were scanned on Bruker-DPX-300 MHz spectrometer in the specified solvent, with TMS and TSP as internal references (specified where necessary). All of the chemical shifts are reported in parts per million (δ ppm). Coupling constants (*J*) are given in Hertz. Proton spectral multiplicities are abbreviated as – s: singlet, d: doublet, t: triplet, m: multiplet, q: quartet, dd: doublet of doublets. High resolution mass spectra (HRMS) were recorded with a Xevo G2-S Q Tof (Waters, USA) instrument by directly injecting the sample dissolved in 2 mL of methanol.
Molar conductivities were measured using TIMPL Auto Ranging Digital Conductivity/TDS Meter TCM-15 of a 10^{-3} M solution in DMSO for temperatures ranging from 10-60°C.
The fluorescence spectra were recorded on the Perkin Elmer LS 55 Fluorescence spectrometer in the range of 200–800 nm for the solutions of the compounds dissolved in DMSO.

General procedure for synthesis of 2-arylimidazo[1,2-*a*]pyridines (12b-d)-Aminopyridine (1.5g, 15.9 mmol), phenacyl bromide or *p*-substituted phenacyl bromide (15.9 mmol) and triethylamine (4.3 mL, 31.8 mmol, 2 equiv.) were dissolved in THF (5 mL) and 4Å molecular sieves (0.1 mol %) were added to the reaction mixture. It was refluxed at 50-55°C for 6 hours. The progress of the reaction was monitored using TLC (hexane:ethyl acetate, 1:1 v/v). After completion of the reaction, the product was filtered over a sintered funnel. The filtrate was concentrated, and the product was purified by column chromatography over silica gel. The product was recrystallized from hot ethanol.

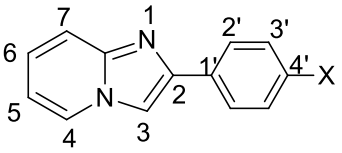

12	b	c	d
X	H	OCH_3	NO_2

2-Phenylimidazo[1,2-*a*]pyridine (12b).Yellow solid (78%); mp 129-130°C; IR (KBr) ν_{max} cm^{-1} 3128, 3036, 1624, 1462, 1362, 1254; ^{1}H NMR (400 MHz, CD_3CN) δ 6.78 (t, $^3J_{HH}$ 6.8 Hz, 1H, H5), 7.17 (t, $^3J_{HH}$ 8.0Hz, 1H, H6), 7.27–7.29 (unresolved m, 5H, H2',H3',H4'), 7.93 (d, $^3J_{HH}$ 7.6Hz, 1H, H7), 8.07 (s, 1H, H3), 8.27(d, $^3J_{HH}$ 6.8Hz, 1H, H4).

2-(4-Methoxyphenyl)imidazo[1,2-*a*]pyridine (12c). Light brown solid (87%); mp 137-138°C; IR (KBr) ν_{max} cm^{-1} 3065, 2947, 2854, 1486, 1251; ^{1}H NMR (400 MHz, d_6-DMSO) δ3.72(s, 3H, OCH_3, H16), 6.76 (t, $^3J_{HH}$ 6.2Hz, 1H, H5), 6.90 (d, $^3J_{HH}$ 8.8Hz, 2H, H3'), 7.11 (t, $^3J_{HH}$ 8.4Hz, 1H, H6), 7.43 (d, J_{HH} 9.2Hz, 1H, H7), 7.78 (d, $^3J_{HH}$ 8.8Hz, 2H, H2'), 8.18 (s, 1H, H3), 8.39 (d, $^3J_{HH}$ 7.2Hz, 1H, H4).

2-(4-Nitrophenyl)imidazo[1,2-*a*]pyridine (12d). Brown solid (68%); mp 260-261°C; IR (KBr) ν_{max} cm^{-1} 2965, 2821, 1597, 1511, 1261, 1200; ^{1}H NMR (400 MHz, $CDCl_3$) δ 6.89 (t, $^3J_{HH}$ 6.8Hz, 1H, H5), 7.29 (t, $^3J_{HH}$ 8.0Hz, 1H, H6), 7.74 (d, $^3J_{HH}$ 8.8Hz 1H, H7), 7.99 (s, 1H, H3), 8.08 (d, $^3J_{HH}$ 8.4Hz, 2H, H2'), 8.16 (d, $^3J_{HH}$ 6.8Hz, 1H, H4), 8.26 (d, $^3J_{HH}$ 8.4Hz, 2H, H3').

Reaction of maleic anhydride (13) with imidazo[1,2-*a*]pyridines (12a-d). Oven-dried glassware was used, and the experiment was carried out at room temperature. To imidazo[1,2-*a*]pyridine (1.7 mmol, **12a** = 200 mg; **12b** = 330 mg; **12c** = 407 mg; **12d** = 381 mg) dissolved in acetonitrile (5 mL) in a 25-mL round bottom (RB) flask, a solution of maleic anhydride (324 mg, 3.3 mmol, 2 equiv.) in acetonitrile (5 mL) was added drop-wise very slowly under stirring using a dropping funnel. After completion of the reaction, the stirring was continued for 24 h. The dark-coloured solid which separated out was filtered, washed with diethyl ether (3 x 5 mL), and dried *in vacuo*.

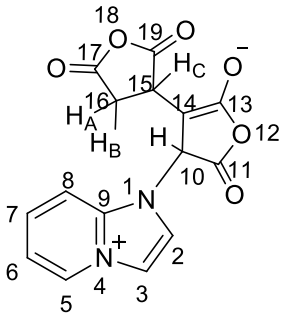

16

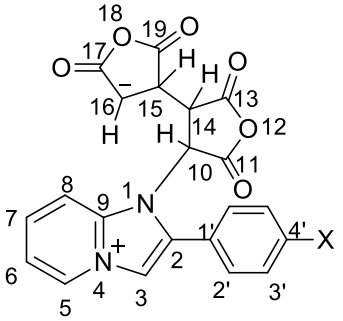

15	b	c	d
X	H	OCH_3	NO_2

3-(2,5-Dioxotetrahydrofuran-3-yl)-4-(1H-imidazo[1,2-*a*]pyridin-4-ium-1-yl)-5-oxo-4,5-dihydrofuran-2-olate (16). Greenish-grey solid (81%); mp 211-212°C; IR (KBr) ν_{max} cm^{-1} 3436, 2501, 1725, 1661, 1321, 1238, 760; ^{1}H NMR (300 MHz, D_2O+TSP) δ 3.30 (dd, $^2J_{HH}$ 17.2Hz, $^3J_{HH}$ 9.6Hz, 1H, H16a), 3.44 (dd, $^2J_{HH}$ 17.2Hz, $^3J_{HH}$ 4.8Hz, 1H, H16b), 5.69 (dd, $^2J_{HH}$ 9.6Hz, $^3J_{HH}$ 4.8Hz, 1H, H15), 7.49 (dd, $^2J_{HH}$ 8.2Hz, $^3J_{HH}$ 3.0Hz, 1H, H6), 8.01 (merged doublets, 2H, H7, H3), 8.07 (d, $^5J_{HH}$ 1.8Hz, 1H, H2), 8.15 (d, $^5J_{HH}$ 1.8Hz, 1H, H8), 8.69 (d, $^3J_{HH}$ 6.8Hz, 1H, H5); ^{13}C NMR (125MHz, d_6-DMSO) δ36.7, 55.9, 111.6, 112.6, 113.3, 115.1, 116.1, 117.2, 124.5, 125.5, 127.2, 129.6, 131.5, 133.7, 139.1, 167.0, 168.7, 170.9. HRMS (*m/z*): $C_{15}H_{10}N_2O_6$ 314.2497, calc for (M+H): 315.2576, found 315.2570.

4-(2,5-Dioxo-4-(2-phenyl-1H-imidazo[1,2-*a*]pyridin-4-ium-1-yl)tetrahydrofuran-3-yl)-2,5-dioxotetrahydrofuran-3-ide (15b). Dark brown solid (84%); mp 159-160°C; IR (KBr) ν_{max} cm^{-1} 3102, 2888, 1782, 1590, 1445, 1044; ^{1}H NMR (300 MHz, D_2O+TSP) δ 3.67 (unresolved d, 1H, H16), 3.82 (unresolved t, 1H, H15), 4.04 (t, $^3J_{HH}$ 9.0 Hz, 1H, H14), 4.21 (d, $^3J_{HH}$ 8.8Hz, 1H, H10), 7.35 (t, $^3J_{HH}$ 6.9 Hz, 1H, H4'), 7.57 (m, 3H, H6, H7, H8), 7.82 (d,$^3J_{HH}$ 4.2Hz, 2H, H3'), 7.87 (d, $^3J_{HH}$ 7.3Hz, 2H, H2'), 8.33 (s, 1H, H3), 8.61 (d, $^3J_{HH}$ 6.6Hz, 1H, H5); ^{13}C NMR (75 MHz, d_6-DMSO) δ109.9, 114.2, 114.9, 125.8, 127.7, 128.2, 128.7, 129.0, 131.1, 131.8, 141.0, 143.1, 166.8. HRMS (*m/z*): $C_{21}H_{14}N_2O_6$ 390.3457, calc for (M+H): 391.3536, found 391.3456.

4-(4-(2-(4-Methoxyphenyl)-1H-imidazo[1,2-*a*]pyridin-4-ium-1-yl)-2,5-dioxotetrahydrofuran-3-yl)-2,5-dioxotetrahydrofuran-3-ide (15c). Brown solid (85%) ; mp 260-261°C; IR (KBr) ν_{max} cm^{-1} 3098, 2964, 1723, 1597, 1259, 1178, 1023; ^{1}H NMR (400 MHz, d_6-DMSO) δ 3.00-3.50 (merged with the solvent peak, 4H, H10, H14, H15, H16), 6.07 (s, 3H, $OC\underline{H}_3$), 6.97 (m, 3H, H6, H3'), 7.39 (t, $^3J_{HH}$ 7.8Hz, 1H, H7), 7.59 (d, $^3J_{HH}$ 7.8Hz, 1H, H8), 7.78 (d, $^3J_{HH}$ 8.4Hz, 2H, H2'), 8.34 (s, 1H, H3), 8.53 (d, $^3J_{HH}$ 6.8Hz, 1H, H5); ^{13}C NMR (100 MHz, d_6-DMSO) δ55.8, 109.3, 114.6, 114.9, 115.1, 127.8, 128.1, 128.5, 133.2, 160.2, 167.4, 211.4. HRMS (*m/z*): $C_{22}H_{16}N_2O_7$ 420.3716, calc for (M+H): 421.3796, found 421.3771.

4-(4-(2-(4-Nitrophenyl)-1H-imidazo[1,2-*a*]pyridin-4-ium-1-yl)-2,5-dioxotetrahydrofuran-3-yl)-2,5-dioxotetrahydrofuran-3-ide (15d). Light brown solid (82%); mp (decomposes at) 286-287°C; IR (KBr) ν_{max} cm^{-1} 3119, 2962, 1521, 1453, 1347, 1099, 1026; ^{1}H NMR (400 MHz, d_6-DMSO) δ 3.00-3.50 (merged with the solvent peak, 4H, H10, H14, H15, H16), 6.86 (t, $^3J_{HH}$ 6.4Hz, 1H, H6), 7.23 (t, $^3J_{HH}$ 8.0Hz, 1H, H7), 7.53 (d, $^3J_{HH}$ 8.8Hz, 1H, H8), 8.17 (dd, $^2J_{HH}$ 25.2Hz, $^3J_{HH}$ 8.4Hz, 4H, H2', H3'), 8.48 (d, $^3J_{HH}$ 6.8Hz, 1H, H5), 8.56 (s, 1H, H3); ^{13}C NMR (100 MHz, d_6-DMSO) δ100.8, 117.4, 122.6, 124.7, 126.8, 127.8, 145.6, 146.9, 181.3. HRMS (*m/z*): $C_{21}H_{13}N_3O_8$ 435.3432, calc for (M+H): 436.3512, found 437.0878.

Computational methods

All of the calculations were done using Gaussian16 suite of programs. All of the geometries were optimized at B3LYP/6-31+G(d) level of theory. Frequency calculations were done at the same level to identify the global minimum or the first saddle point having zero or one imaginary frequency, respectively. Intrinsic reaction coordinate (IRC) calculations were done to correlate the transition states to their respective reactants and products. TDDFT calculations were done at wB97XD/6-311+G(d,p) level. The thermodynamic data and Cartesian coordinates of relevant structures are given in SM.

Acknowledgements

The authors thankfully acknowledge the research facilities provided by the authorities of the IIS (deemed to be University), Jaipur, Macleods Pharmaceuticals, Mumbai and Panjab University, Chandigarh, India for recording the NMR and HRMS data.

Supplementary Material

The ^{1}H, ^{13}C, 2D-NMR spectra, HRMS are provided as supplementary material in the online version.

References

1. Ollis, W.D.; Stanforth, S.P.; Ramsden, C.A. *Tetrahedron* **1985**, *41*, 2239. https://doi.org/10.1016/S0040-4020(01)96625-6
2. Potts, K. T.; Murphy, P. M.; Kuehnling, W.R. *J. Org. Chem*. **1988**, *53*, 2889. https://doi.org/10.1021/jo00248a003
3. Ramsden, C.A. *Tetrahedron* **2013**, *69*, 4146. https://doi.org/10.1016/j.tet.2013.02.081
4. Bobeck, D.R.; Lee, H.I. ; Flick, A.C. ; Padwa, A. *J. Org. Chem*. **2009**, *74*, 7389. https://doi.org/10.1021/jo901336z
5. Nachaev, I.V.; Cherkaev, G.V. ; Sheremetev, A.B. *J. Org. Chem*. **2022**, *87*, 652. https://doi.org/10.1021/acs.joc.1c02630
6. Zhang, J.; Xu, W.; Sheng, P. ; Zhao, G. ; Zhu, D. *Acc. Chem. Res.* **2017**, 50, 1654. https://doi.org/10.1021/acs.accounts.7b00124
7. Diels, O.; Alder, K. *Liebigs Ann. Chem*. **1932,** *498*, 16. https://doi.org/10.1002/jlac.19324980103
8. Acheson, R.M.; Taylor, G.A. *J. Chem. Soc.* **1960**, 1691. https://doi.org/10.1039/JR9600001691
9. Kamienska-Trela, K.; Raynes, W.T.; Taylor, B.F. *Magn. Reson. Chem.* **1987**, *25*, 396. https://doi.org/10.1002/mrc.1260250503
10. Huisgen, R.; Herbig, K. *Liebigs Ann. Chem.*, **1965**, *688*, 98. https://doi.org/10.1002/jlac.19656880112
11. Aginagalde, M.; Vara, Y.; Arrieta, A.; Zangi, R.; Cebolla, V.L.; Delgado-Camin, A.; Cossio, F.P. *J. Org. Chem.* **2010**, *75*, 2776. https://doi.org/10.1021/jo9022815
12. Sharma, N.; Kour, M.; Gupta, R.; Bansal, R. K. *RSC Adv*. **2021**, *11*, 25296. https://doi.org/10.1039%2Fd1ra03981d
13. Eickmans, J.; Bieringer,T.; Kostromine, S.; Berneth, H.; Thoma, J. *Jpn. J. Appl. Phys*. **1999**, *1*, 1835. https://doi.org/10.1143/JJAP.38.1835
14. Theis, A.; Ritter, H.; Bhme, C. Klinger, Mittler, S.; Menges, *B. Chem. Mater*. **2002**, *14*, 2109. https://doi.org/10.1021/cm011230v
15. Das, R.; Majumdar, N.; Lahiri, A. *Int. J. Res. Pharm. Chem*. **2014**, *4*, 467. http://dx.doi.org/10.1002/chin.201507324
16. Rival, Y.; Grassy, G.; Michel, G. *Chem. Pharm. Bull.* **1992**, *40*, 1170. (and references cited therein)

https://doi.org/10.1248/cpb.40.1170
17. Deutschmann, T.; Ritter, H. *Macromol. Chem. Phys.* **2000**, *201*, 1200. https://doi.org/10.1002/1521-3935(20000701)201:11%3C1200::AID-MACP1200%3E3.0.CO;2-2
18. Neochoritis, C. G.; Zarganes-Tzitzikas, T.; Stephanidou-Stephanatou, J. *Synthesis* **2014**, *46*, 537. https://doi.org/10.1055%2Fs-0033-1340615
19. Tallon, M. A. *Reactions Involving Maleic Anhydride. In: Musa, O. (eds) Handbook of Maleic Anhydride Based Materials*; Springer, Cham, 2016; pp 59–149. https://doi.org/10.1007/978-3-319-29454-4_2
20. Cookson, R.C; Isaacs, N. S. *Tetrahedron* **1963**, *19*, 1237. https://doi.org/10.1016/S0040-4020(01)98585-0
21. GaussView, Version 6, Dennington, Roy; Keith, Todd A.; Millam, John M. Semichem Inc., Shawnee Mission, KS, 2016.
22. Politzer, P. ; Daiker, K. C. *Models for Chemical Reactivity In The Force Concept in Chemistry*, *ed. R. C. Deb;* Van Nostrand Reinhold Co., New York, 1981. https://doi.org/10.1103/RevModPhys.45.22
23. Tasi, G.; Palinko, I.; Nyerges, L.; Fejes, P.; Forster, H. *J. Chem. Inf. Comput. Sci.* **1993**, *33*, 296. https://doi.org/10.1021/ci00013a003
24. Pidlypnyi, N.; Kaul, S.; Wolf, S.; Drafz, M. H. H.; Schmidt, A. *Z. Naturforsch. B* **2014**, *69b*, 605. https://doi.org/10.5560/znb.2014-3324
25. Grabowski, Z.; R. Rotkiewicz K.; Rettig W. *Chem. Rev.* **2003**, *103*, 3899. https://doi.org/10.1021/cr940745l
26. Siemiarczuk, A.; Grabowski, Z. R.; Krówczyński, A.; Asher, M.; Ottolenghi, M. *Chem. Phys. Lett.* **1977**, *51*, 315. https://doi.org/10.1016/0009-2614(77)80411-9
27. Naito, T. *Crystals* **2021**, *11*, 838. https://doi.org/10.3390/cryst110
28. Sinha, H. K.; Muralidharan, S.; Yates, K. *Can. J. Chem.* **1992**, *70*, 1932. https://doi.org/10.1139/v92-242
29. Wheland, R.C.; Gillson, J. L. *J. Am. Chem. Soc.* **1976**, *98*, 3916. https://doi.org/10.1021/ja00429a030
30. Wheland, R.C. *J. Am. Chem. Soc.* **1976**, *98,* 3926. https://doi.org/10.1021/ja00429a031
31. Mori, T.; Kawamoto, T. *Annu. Rep. Prog. Chem., Sect. C: Phys. Chem.* **2007**,*103*, 134. https://doi.org/10.1039/B605647B
32. Zobel, D.; Ruban, G. *Acta Cryst.* **1983,** *B39*, 638. https://doi.org/10.1107/S0108768183003092
33. Grabowski, Z. R.; Rotkiewicz, K.; Rettig, W. *Chem. Rev.* **2003,** *103*, 3899. https://doi.org/10.1021/cr940745l
34. Brittinger, C.; Maiti, A. K.; Baumann, W.; Detzer, N. *Z. Naturforsch. A* **1990**, *45a*, 883. https://doi.org/10.1515/zna-1990-0708
35. Russell, T. D.; Levy, D. H. *J. Phys. Chem.* **1982**, *86*, 2718. https://doi.org/10.1021/j100211a033
36. Phillips, S. M.; Smith, G. D. *J. Phys. Chem. A* **2015**, *119*, 4545. https://doi.org/10.1021/jp510709e

37. Chen, M-C.; Chen, D-G.; Chou, P-T. *ChemPlusChem* **2020**, *86*, 11. https://doi.org/10.1002/cplu.202000592
38. Mostafa, A.; Bazzi, H. S. *Spectrochim. Acta, Part A.* **2009**, *74*, 180. https://doi.org/10.1016/j.saa.2009.06.004
39. Alghanmi, R. M.; Habeeb, M. M. *J. Mol. Liq.* **2013**, *181*, 20. https://doi.org/10.1016/j.molliq.2013.02.007
40. Adamo, C.; Jacquemin, D. *Chem. Soc. Rev.* **2013**, *42*, 845. https://doi.org/10.1039/C2CS35394F
41. Le Bahers, T.; Adamo, C.; Ciofini, I. *J. Chem. Theory Comput*. **2011**, *7*, 2498. https://doi.org/10.1021/ct200308m
42. Ciofini, I.; Le Bahers, T.; Adamo, C.; Odobel, F.; Jacquemin, D. *J. Phys. Chem. C.* **2012**, *116*, 11946. https://doi.org/10.1021/jp3030667
43. Dreuw, A.; Head-Gordon, M. *J. Am. Chem. Soc.* **2004**, *126*, 4007. https://doi.org/10.1021/ja039556n
44. **Gaussian 16** Calculations Suite: Frisch, M. J.; Trucks, G. W.; Schlegel, H. B.; Scuseria, G. E.; Robb, M. A.; Cheeseman, J. R.; Scalmani, G.; Barone, V.; Petersson, G. A.; Nakatsuji, H.; Li, X.; Caricato, M.; Marenich, A. V.; Bloino, J.; Janesko, B. G.; Gomperts, R.; Mennucci, B.; Hratchian, H. P.; Ortiz, J. V.; Izmaylov, A. F.; Sonnenberg, J. L.; Williams-Young, D.; Ding, F.; Lipparini, F.; Egidi, F.; Goings, J.; Peng, B.; Petrone, A.; Henderson, T.; Ranasinghe, D.; Zakrzewski, V. G.; Gao, J.; Rega, N.; Zheng, G.; Liang, W.; Hada, M.; Ehara, M.; Toyota, K.; Fukuda, R.; Hasegawa, J.; Ishida, M.; Nakajima, T.; Honda, Y.; Kitao, O.; Nakai, H.; Vreven, T.; Throssell, K.; Montgomery, J. A., Jr.; Peralta, J. E.; Ogliaro, F.; Bearpark, M. J.; Heyd, J. J.; Brothers, E. N.; Kudin, K. N.; Staroverov, V. N.; Keith, T. A.; Kobayashi, R.; Normand, J.; Raghavachari, K.; Rendell, A. P.; Burant, J. C.; Iyengar, S. S.; Tomasi, J.; Cossi, M.; Millam, J. M.; Klene, M.; Adamo, C.; Cammi, R.; Ochterski, J. W.; Martin, R. L.; Morokuma, K.; Farkas, O.; Foresman, J. B.; Fox, D. J. Gaussian, Inc., Wallingford CT, **2016**.